Electron acceleration by tightly focused radially polarized few-cycle laser pulses*

Liu Jin-Lu(刘晋陆), Sheng Zheng-Ming(盛政明)†, and Zheng Jun(郑 君)

Key Laboratory for Laser Plasmas (Ministry of Education) and Department of Physics, Shanghai Jiao Tong University, Shanghai 200240, *China*

(Received 10 May 2011; revised manuscript received 19 August 2011)

Within the framework of plane-wave angular spectrum analysis of the electromagnetic field structure, a solution valid for tightly focused radially polarized few-cycle laser pulses propagating in vacuum is presented. The resulting field distribution is significantly different from that based on the paraxial approximation for pulses with either small or large beam diameters. We compare the electron accelerations obtained with the two solutions and find that the energy gain obtained with our new solution is usually much larger than that with the paraxial approximation solution.

Keywords: radially polarized laser pulses, few-cycle pulses, plane-wave angular spectrum analysis, direct laser acceleration of electrons

PACS: 41.75.Jv, 42.25.Bs **DOI:** 10.1088/1674-1056/21/2/024101

1. Introduction

Recent development in the chirped pulse amplification (CPA) laser technology has enabled one to obtain ultra-intense ($\sim 10^{22}$ W/cm^2) and ultra-short (few-cycle or sub-cycle) lasers.[1,2] Such lasers may provide ultra-high acceleration gradients for charged particles, e.g., a few orders of magnitude higher than conventional accelerators. Recently it was proposed to accelerate electrons in a vacuum using radially polarized intense laser beams.[3−6] It shows some advantages over normal Gaussian laser beams because of its stronger longitudinal field. Most existing studies[7−11] are, however, based on the paraxial approximation (PA), which is correct only for relatively large waist spot size. At the same time, since ultra-short especially few-cycle or sub-cycle laser pulses have strong coupling in the spatial and the temporal profiles during propagation, one must consider these important effects in calculating electron energy gain by such laser pulses.[12−14]

In this paper, we present a non-paraxial solution for the propagation of radially polarized laser pulse in vacuum according to the plane-wave angular spectrum analysis (ASA) of the electromagnetic field structure. For the temporal profile, we calculate the field up to the second order in $O[1/(\omega_0 t_0)^2]$. Using this solution, the electron acceleration by a radially polarized laser pulse in a vacuum is investigated numerically. The results are compared with those obtained with the paraxial approximation PA solution.

2. Non-paraxial solution of radially polarized ultrashort laser pulses

Within the framework of plane-wave ASA,[15−17] the electromagnetic fields of radially polarized laser are described as follows:[4−6,18]

$$E_r(R,\theta,z,\omega) = 2\pi\,\mathrm{i}\int_0^1 b(\omega,\rho)\sqrt{1-\rho^2}\mathrm{J}_1\left(\frac{\omega}{c}R\rho\right) \times \exp\left(\mathrm{i}\frac{\omega}{c}z\sqrt{1-\rho^2}\right)\rho\mathrm{d}\rho, \quad (1)$$

$$E_z(R,\theta,z,\omega) = -2\pi\int_0^1 b(\omega,\rho)\rho\mathrm{J}_0\left(\frac{\omega}{c}R\rho\right) \times \exp\left(\mathrm{i}\frac{\omega}{c}z\sqrt{1-\rho^2}\right)\rho\mathrm{d}\rho, \quad (2)$$

$$B_\theta(R,\theta,z,\omega) = 2\pi\,\mathrm{i}\int_0^1 b(\omega,\rho)\mathrm{J}_1\left(\frac{\omega}{c}R\rho\right) \times \exp\left(\mathrm{i}\frac{\omega}{c}z\sqrt{1-\rho^2}\right)\rho\mathrm{d}\rho, \quad (3)$$

where $b(\omega,\rho) = A\rho\exp(-\rho^2/4\sigma^2)\mathrm{L}_n^1(\rho^2/2\sigma^2)/\sqrt{1-\rho^2}$, $A = (-1)^{n+1}\sqrt{2}\,\mathrm{i}\,E_0/(8\pi\sigma^3)$, $\sigma = 1/(kw) = c/(\omega w)$, L_n^1 is the associated Laguerre polynomials of the radial mode number n and the angular mode number

*Project supported by the National Natural Science Foundation of China (Grant Nos. 10734130, 10935002, and 11075105) and the National Basic Research Program of China (Grant No. 2009GB105002).

†Corresponding author. E-mail: zmsheng@sjtu.edu.cn

© 2012 Chinese Physical Society and IOP Publishing Ltd

1, we set $n = 0$ throughout this paper. J_0 and J_1 refer to the Bessel functions of the first kind of order 0 and 1, respectively. E_0 is an arbitrary amplitude constant. w is the beam waist spot size, ω is the plane wave component frequency, ρ is the planar polar coordinates related to the Cartesian Fourier transform as defined in Refs. [4] and [5]. The exact expression of a radially polarized laser pulse can be written as

$$F(R,\theta,z,t) = \int_{-\infty}^{+\infty} \tilde{f}(\omega-\omega_0)\hat{F}(R,\theta,z,\omega) \times \exp(-\mathrm{i}\,\omega\tau)\,\mathrm{d}\omega,$$

where $\tau = t - z/c$, ω_0 is the central angular frequency, $\hat{F} = \hat{E}_r, \hat{E}_z, \hat{B}_\theta$ and the corresponding components of $\hat{F}(R,\theta,z,\omega)$ are

$$\hat{E}_r(R,\theta,z,\omega) = 2\pi\,\mathrm{i}\int_0^1 b(\omega,\rho)\sqrt{1-\rho^2}\mathrm{J}_1\left(\frac{\omega}{c}R\rho\right) \times \exp\left[\mathrm{i}\,\frac{\omega}{c}z(\sqrt{1-\rho^2}-1)\right]\rho\mathrm{d}\rho, \quad (4)$$

$$\hat{E}_z(R,\theta,z,\omega) = -2\pi\int_0^1 b(\omega,\rho)\rho\mathrm{J}_0\left(\frac{\omega}{c}R\rho\right) \times \exp\left[\mathrm{i}\,\frac{\omega}{c}z(\sqrt{1-\rho^2}-1)\right]\rho\mathrm{d}\rho, \quad (5)$$

$$\hat{B}_\theta(R,\theta,z,\omega) = 2\pi\,\mathrm{i}\int_0^1 b(\omega,\rho)\mathrm{J}_1\left(\frac{\omega}{c}R\rho\right) \times \exp\left[\mathrm{i}\,\frac{\omega}{c}z(\sqrt{1-\rho^2}-1)\right]\rho\mathrm{d}\rho. \quad (6)$$

Following Refs. [7], [17], [19]–[21], assuming that $\hat{F}(R,\theta,z,\omega)$ is a slowly varying function of ω with respect to the $\mathrm{e}^{-\mathrm{i}\,\omega t}$ term, $\tilde{f}(\omega-\omega_0)$ sharply peaks around ω_0, one can evaluate Eqs. (4), (5) and (6) using the Taylor expansion:

$$\begin{aligned} &F(R,\theta,z,t) \\ &= \sum_{n=0}\frac{1}{n!}\frac{\partial^n\hat{F}(R,\theta,z,\omega)}{\partial\omega^n}\Big|_{\omega=\omega_0}\exp(-\mathrm{i}\,\omega_0\tau) \\ &\quad\times\int_{-\infty}^{+\infty}\tilde{f}(\omega-\omega_0)(\omega-\omega_0)^n \\ &\quad\times\exp[-\mathrm{i}(\omega-\omega_0)\tau]\,\mathrm{d}\omega. \end{aligned} \quad (7)$$

Adopt the Gaussian spectral distribution: $\tilde{f}(\omega-\omega_0) = t_0\exp[-(\omega-\omega_0)^2t_0^2/2]/\sqrt{2\pi}$, where t_0 is the laser pulse duration and assume that the waist spot size is the same for all the spectral components of the pulse, then one can obtain

$$\begin{aligned} F(R,\theta,z,t) &= \hat{F}(R,\theta,z,\omega_0)\exp(-\mathrm{i}\,\omega_0\tau)\exp(-\tau^2/2t_0^2) \\ &\quad+\frac{\partial\hat{F}(R,\theta,z,\omega)}{\partial\omega}\Big|_{\omega=\omega_0}\exp(-\mathrm{i}\,\omega_0\tau)(-\mathrm{i}\,\tau/t_0^2)\exp(-\tau^2/2t_0^2) \\ &\quad+\frac{1}{2}\frac{\partial^2\hat{F}(R,\theta,z,\omega)}{\partial\omega^2}\Big|_{\omega=\omega_0}\exp(-\mathrm{i}\,\omega_0\tau)(1/t_0^2)(1-\tau^2/t_0^2)\exp(-\tau^2/2t_0^2)+\cdots. \end{aligned} \quad (8)$$

Notice that the n-th term in Eq. (8) scales as $1/(\omega_0t_0)^n$, which is a small quantity as long as $t_0 \gg 1/\omega_0$. With the help of

$$\frac{\partial b(\omega,\rho)}{\partial\omega} = \frac{(-1)^{n+1}\sqrt{2}\,\mathrm{i}\,E_0}{8\pi c^3}\frac{\rho}{\sqrt{1-\rho^2}}\left(3\omega^2w_0^3-\frac{\rho^2}{2c^2}\omega^4w_0^5\right)\exp\left(-\frac{\rho^2}{4\sigma^2}\right), \quad (9)$$

$$\frac{\partial^2 b(\omega,\rho)}{\partial\omega^2} = \frac{(-1)^{n+1}\sqrt{2}\,\mathrm{i}\,E_0}{8\pi c^3}\frac{\rho}{\sqrt{1-\rho^2}}\left(6\omega w_0^3-\frac{7\rho^2}{2c^2}\omega^3w_0^5+\frac{\rho^4}{4c^4}\omega^5w_0^7\right)\exp\left(-\frac{\rho^2}{4\sigma^2}\right), \quad (10)$$

one can obtain the second-order temporally corrected fields as

$$\begin{aligned} E_r(R,\theta,z,t) &= 2\pi\,\mathrm{i}\left[\int_0^1\sqrt{1-\rho^2}b(\omega,\rho)\mathrm{J}_1(Q)\exp(T)\rho\mathrm{d}\rho+\int_0^1\sqrt{1-\rho^2}G_1\exp(T)\rho\mathrm{d}\rho(-\mathrm{i}\,\tau/t_0^2)\right. \\ &\quad\left.+\frac{1}{2}\int_0^1\sqrt{1-\rho^2}G_2\exp(T)\rho\mathrm{d}\rho\times(1/t_0^2)(1-\tau^2/t_0^2)\right]\exp(-\tau^2/2t_0^2), \end{aligned} \quad (11)$$

$$\begin{aligned} E_z(R,\theta,z,t) &= -2\pi\left[\int_0^1\rho b(\omega,\rho)\mathrm{J}_0(Q)\exp(T)\rho\mathrm{d}\rho+\int_0^1\rho G_3\exp(T)\rho\mathrm{d}\rho(-\mathrm{i}\,\tau/t_0^2)\right. \\ &\quad\left.+\frac{1}{2}\int_0^1\rho G_4\exp(T)\rho\mathrm{d}\rho\times(1/t_0^2)(1-\tau^2/t_0^2)\right]\exp(-\tau^2/2t_0^2), \end{aligned} \quad (12)$$

$$\begin{aligned} B_\theta(R,\theta,z,t) &= 2\pi\,\mathrm{i}\left[\int_0^1 b(\omega,\rho)\mathrm{J}_1(Q)\exp(T)\rho\mathrm{d}\rho+\int_0^1 G_1\exp(T)\rho\mathrm{d}\rho(-\mathrm{i}\,\tau/t_0^2)\right. \\ &\quad\left.+\frac{1}{2}\int_0^1 G_2\exp(T)\rho\mathrm{d}\rho(1/t_0^2)(1-\tau^2/t_0^2)\right]\exp(-\tau^2/2t_0^2), \end{aligned} \quad (13)$$

where

$$
\begin{aligned}
G_1 &= \frac{\partial b(\omega,\rho)}{\partial\omega}\mathrm{J}_1(Q)+b(\omega,\rho)\left[\frac{\partial \mathrm{J}_1(Q)}{\partial\omega}+\mathrm{J}_1(Q)A\right],\\
G_2 &= \frac{\partial^2 b(\omega,\rho)}{\partial\omega^2}\mathrm{J}_1(Q)+2\frac{\partial b(\omega,\rho)}{\partial\omega}\frac{\partial \mathrm{J}_1(Q)}{\partial\omega}\\
&\quad +2\mathrm{J}_1(Q)\frac{\partial b(\omega,\rho)}{\partial\omega}A+b(\omega,\rho)\\
&\quad \times\left[\frac{\partial^2 \mathrm{J}_1(Q)}{\partial\omega^2}+2\frac{\partial \mathrm{J}_1(Q)}{\partial\omega}A+\mathrm{J}_1(Q)A^2\right],\\
G_3 &= \frac{\partial b(\omega,\rho)}{\partial\omega}\mathrm{J}_0(Q)+b(\omega,\rho)\left[\frac{\partial \mathrm{J}_0(Q)}{\partial\omega}+\mathrm{J}_0(Q)A\right],\\
G_4 &= \frac{\partial^2 b(\omega,\rho)}{\partial\omega^2}\mathrm{J}_0(Q)+2\frac{\partial b(\omega,\rho)}{\partial\omega}\frac{\partial \mathrm{J}_0(Q)}{\partial\omega}\\
&\quad +2\mathrm{J}_0(Q)\frac{\partial b(\omega,\rho)}{\partial\omega}A+b(\omega,\rho)\\
&\quad \times\left[\frac{\partial^2 \mathrm{J}_0(Q)}{\partial\omega^2}+2\frac{\partial \mathrm{J}_0(Q)}{\partial\omega}A+\mathrm{J}_0(Q)A^2\right],
\end{aligned}
$$

with $\omega=\omega_0$, $Q=\omega_0 R\rho/c$, $T=\mathrm{i}\,\omega_0(z\sqrt{1-\rho^2}/c-t)+\varphi_0$, and $A=\mathrm{i}\,z(\sqrt{1-\rho^2}-1)/c$.

In a few previous studies, a simple PA solution of radially polarized laser pulse has been used,[8,11] which is usually expressed as $\boldsymbol{E}=\hat{r}E_r+\hat{z}E_z$, where

$$
\begin{aligned}
E_r &= E_0\frac{r}{w_0 f^2}\exp\left(-\frac{r^2}{w_0^2 f^2}\right)\cos(\varphi)\\
&\quad\times\exp\left(-\frac{\tau^2}{2t_0^2}\right),\qquad (14)\\
E_z &= E_0\frac{2}{w_0 r_0 f^2}\left[\left(1-\frac{r^2}{w_0^2 f^2}\right)\sin(\phi)\right.\\
&\quad\left.-\frac{z}{z_R}\frac{r^2}{w_0^2 f^2}\cos(\phi)\right]\\
&\quad\times\exp\left(-\frac{r^2}{w_0^2 f^2}\right)\exp\left(-\frac{\tau^2}{2t_0^2}\right),\qquad (15)
\end{aligned}
$$

with $\varphi=\omega t-kz+2\tan^{-1}(z/z_R)-(zr^2)/(z_R w_0^2 f^2)-\varphi_0$, $f^2=1+(z/z_R)^2$, and $z_R=k_0 w_0^2/2$. In the following, we compare the solutions obtained by PA solution and our ASA solution in both field properties and electron acceleration.

In our calculation, length l, time t, velocity $\boldsymbol{v}$, momentum $\boldsymbol{p}$, energy G, electric field strength $\boldsymbol{E}$, magnetic field strength $\boldsymbol{B}$ are normalized by λ_0, $T_0=2\pi/\omega_0$, c, mc, mc^2, $m\omega_0 c/e$, and $m\omega_0 c/e$, respectively.

3. Axial electric fields

As is well known, the PA solution is the sum of successive powers of $\varepsilon=\lambda/\pi w_0$.[12,13] In the case of a radially polarized laser field, E_z is the sum of even powers of ε, E_r, and B_θ each are the sum of odd powers of ε. This method fails when $\varepsilon\geq 1$, $w_0\leq 0.3183\lambda$ because series expansion is no longer correct for $\varepsilon\geq 1$.[3,7] Even for $\varepsilon<1$ when the high order terms are relatively small, one should be cautious when calculating electron motion in intense laser fields because of strong nonlinear effects.

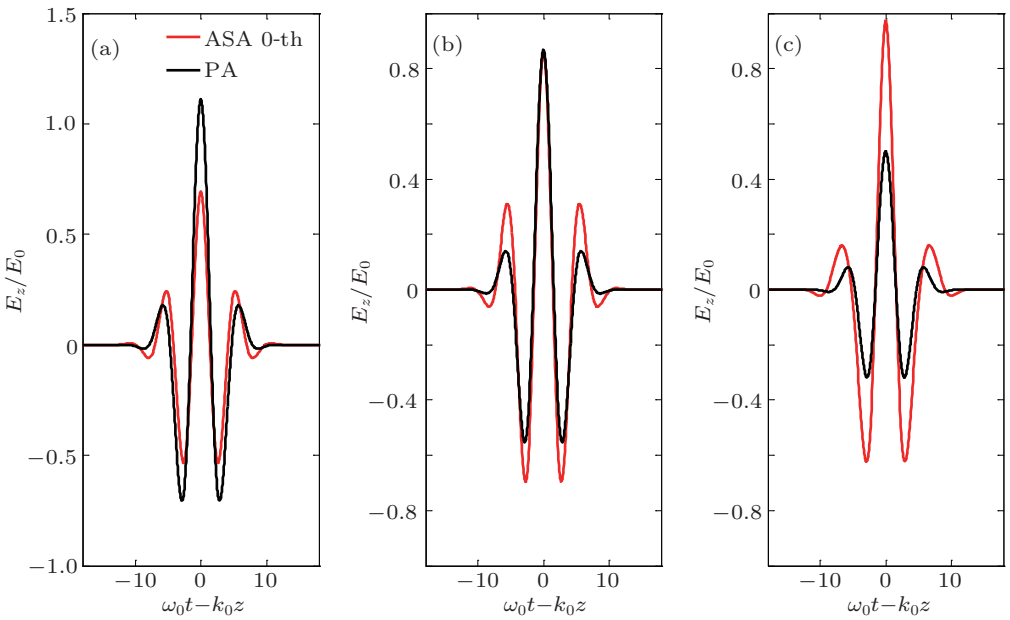


Fig. 1. (colour online) Temporal profiles of the axial electric field E_z of ($t_0=0.5T_0$, $T_0=2\pi/\omega_0$) radially polarized sub-cycle laser pulses each with a Gaussian frequency spectrum at the beam focus ($z=0$). The waist spot sizes are $w_0=0.9\lambda_0/\pi$ (a), $w_0=1.15\lambda_0/\pi$ (b), and $w_0=2\lambda_0/\pi$(c). The initial phase of laser field is $\varphi_0=0.5\pi$. ASA 0-th represents the ASA solution from angular spectrum analysis without higher-order temporal correction. PA represents the paraxial approximation solution.

Figure 1 shows the comparison between the axial electric fields along the laser axis obtained from ASA and PA solutions. It shows that when taking $w_0 < \lambda_0/\pi$, the PA solution is non-physically large since in this case the series expansion in terms of ε is no longer valid; when taking $w_0 = 1.15\lambda_0/\pi$, the ASA solution and the PA solution have almost the same peak. When taking $w_0 = 2\lambda_0/\pi$, our ASA solution predicts a larger axial field than that from the PA solution.

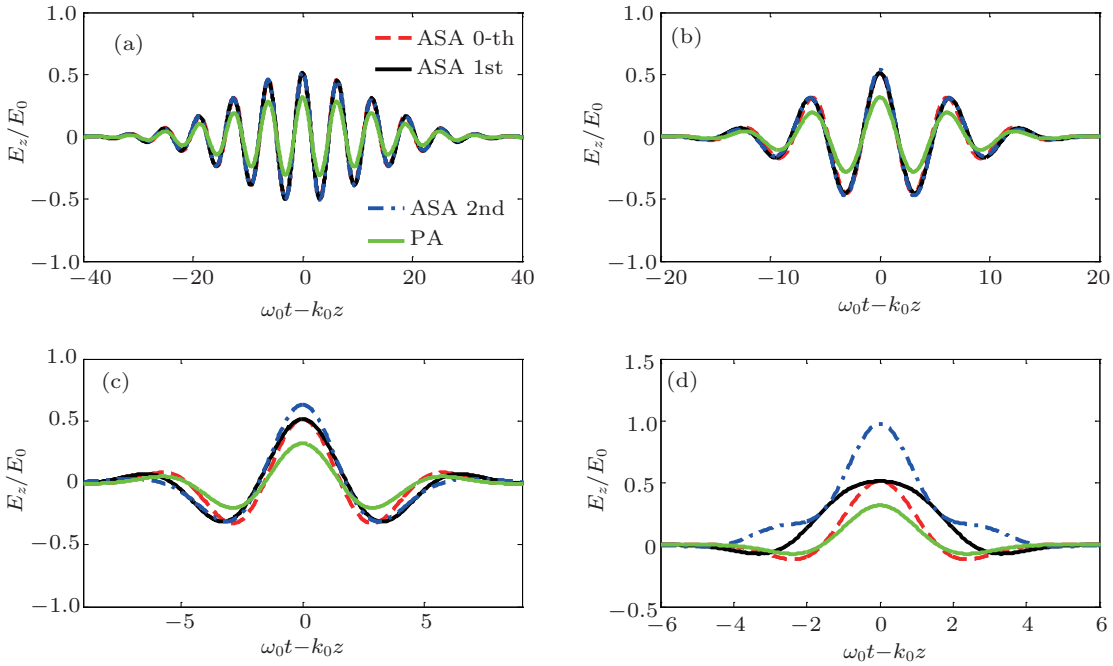


Fig. 2. (colour online) Temporal profiles of the axial electric field E_z of tightly focused ($w_0 = \lambda_0 = 1$ μm) radially polarized ultra-short laser with a Gaussian frequency spectrum at the waist ($z = 0$). The corresponding laser pulse durations are $t_0 = 2T_0$ (a), $t_0 = T_0$ (b), $t_0 = 0.5T_0$ (c), and $t_0 = 0.25T_0$ (d). The initial phase of the field is $\phi_0 = 0.5\pi$. ASA 0-th, ASA 1st, and ASA 2nd represent the ASA solutions with temporal correction to the 0-th order, first order and second order, respectively. PA represents the paraxial approximation.

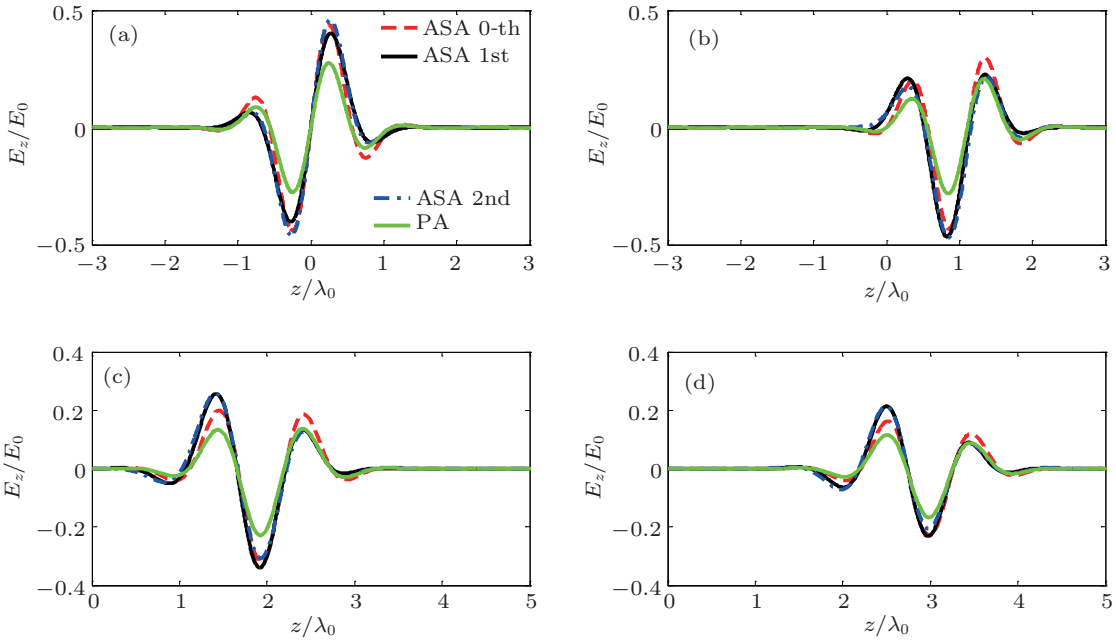


Fig. 3. (colour online) Distributions of the axial electric field E_z of tightly focused ($w_0 = \lambda_0 = 1$ μm) radially polarized ultra-short laser each with a Gaussian frequency spectrum at $t = 0$ (a), $t = T_0$ (b), $t = 2T_0$ (c), and $t = 3T_0$ (d). The initial phase is $\phi_0 = 0.5\pi$ and the laser pulse duration $t_0 = 0.5T_0$. The symbols represent the same meaning as those in Fig. 2.

Figure 2 displays the axial electric fields along the laser axis for various laser pulse durations with a fixed waist spot size radius ($w_0 = \lambda_0$). The ASA solutions give larger values than the PA solutions. When $t_0 > 2T_0$, the high-order temporal correction from Eq. (12) is negligibly small, while when $t_0 < 2T_0$, the high-order correction becomes significantly large. This is obvious since the correction is proportional to $1/t_0$.

Figure 3 shows the axial electric fields along the laser axis at different times with a fixed waist spot size $w_0 = \lambda_0$. The peak electric field of our ASA solution is larger than that of the PA solution. Both solutions show that the field gradually decays with the propagation of the laser pulse out of the focusing region increasing. The difference between ASA solutions with different orders of temporal corrections becomes larger with time. This shows the strong coupling of the spatial and temporal profiles of sub-cycle pulses.

4. Electron acceleration by a radially polarized sub-cycle pulse

The equation of motion for a test electron is given by

$$\mathrm{d}\boldsymbol{p}/\mathrm{d}t = -e(\boldsymbol{E} + \boldsymbol{v} \times \boldsymbol{B}/c).$$

In the dimensionless form, it becomes

$$\mathrm{d}\boldsymbol{p}/\mathrm{d}t = -2\pi(\boldsymbol{E} + \boldsymbol{p} \times \boldsymbol{B}/\gamma),$$

where

$$\gamma = \sqrt{1 + p_z^2}.$$

The equation describing the evolution of electron energy is $\mathrm{d}\gamma/\mathrm{d}t = -2\pi(\boldsymbol{v} \cdot \boldsymbol{E})$. In the cylindrical coordinate system, it leads to

$$\begin{aligned}
&\mathrm{d}p_r/\mathrm{d}t = -2\pi(E_r - v_z B_\phi),\\
&\mathrm{d}p_z/\mathrm{d}t = -2\pi(E_z + v_r B_\phi),\\
&p_z = \gamma v_z,\\
&p_r = \gamma v_r,\ \mathrm{d}r/\mathrm{d}t = p_r/\gamma,\\
&\mathrm{d}z/\mathrm{d}t = p_z/\gamma,\\
&\mathrm{d}\gamma/\mathrm{d}t = -2\pi\boldsymbol{v} \cdot \boldsymbol{E} = -2\pi(v_r E_r + v_z E_z).
\end{aligned}$$

In the following, we discuss the effects of various laser parameters and the initial position of the test electron on electron acceleration. In some simulations,[7–11] the test electron is initially at rest at the origin of the coordinate system, where the transverse fields vanish and the longitudinal field reaches its peak. This electron may move to this position by field ionization of some high Z atoms, for example.

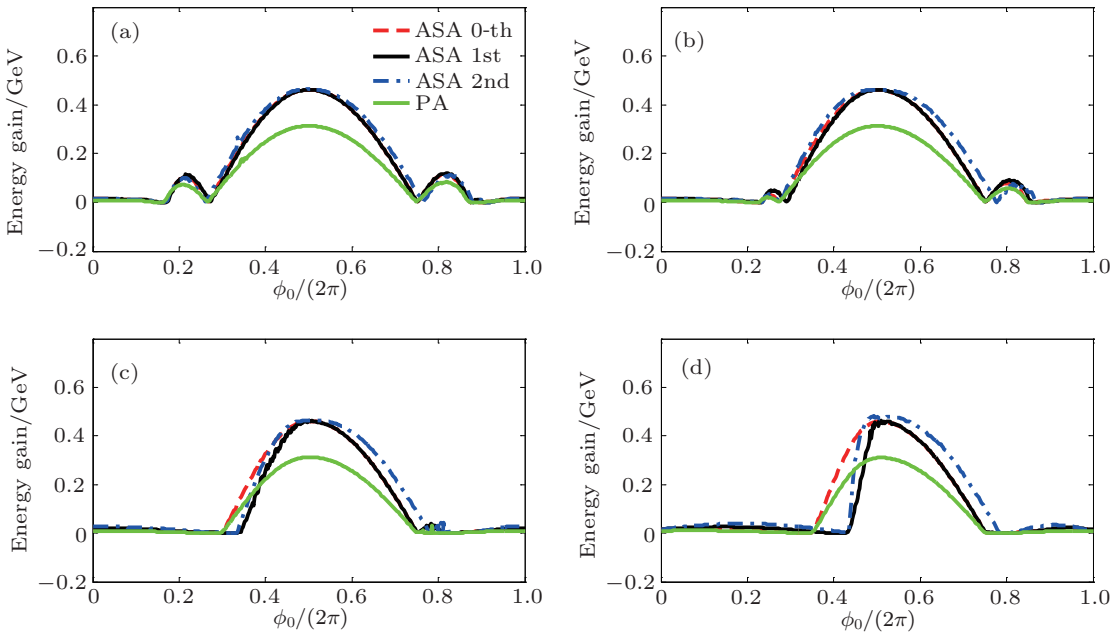


Fig. 4. (colour online) Electron energy gains each as a function of the initial phase ϕ_0 for different pulse durations: $t_0 = 2T_0$ (a), $t_0 = T_0$ (b), $t_0 = 0.5T_0$ (c), and $t_0 = 0.25T_0$ (d). The dimensionless electric field intensity is $E_0 = 100$ and the spot size is $w_0 = \lambda_0 = 1$ μm. The symbols represent the same meanings as those in Fig. 2.

Figure 4 describes the variations of electron energy gain with the initial phase of the laser field ϕ_0 when the test electron is initially located at $z = 0$. It shows that high energy gain is found for the initial phase between $2\pi/3$ and $3\pi/2$. The maximum electron energy gain is at $\phi_0 = \pi$, obtained both with the ASA solution and with the PA solution. This energy peak remains almost the same with or without high-order corrections caused by the temporal profile. This is consistent with existing work, e.g. Refs. [7] and [8]. When $t_0 \leq T_0$, the higher-order corrections modify the electron energy gain to some extent. This can be explained as being due to the coupling of the spatial and the temporal profiles, which modulates the pulse shape during propagation. When the pulse duration is very short such as $t_0 = 0.25T_0$, there is significant difference between the energy gain obtained with the ASA solution and that obtained with the PA solution. One should notice that the electron energy gain obtained with the ASA solution is larger than that obtained with the PA solution. This can be understood from Figs. 1–3, which show that the axial electric field intensity of ASA solution is larger than that of PA solution as long as the beam waist size is not too small.

Figure 5 indicates the variations of electron energy gain with the laser beam waist size w_0, showing that the electron energy gain increases with the beam waist w_0 increasing until it reaches the maximum value (around $w_0 \approx 5\lambda_0$). Then it decreases with the further increase of w_0. This observation is valid for different pulse durations. This results from the following two competing effects: a larger beam waist can provide a longer acceleration distance for a longer Rayleigh length, whereas a large beam waist leads to a smaller axial field for acceleration. Therefore there exists an optimal value of w_0 balancing those two contradictory factors to produce the maximum energy gain. One notices that when $t_0 \leq T_0$, the higher-order corrections can also modify the electron energy gain and the optimal w_0 of higher-order case is slightly larger than those of low-order case. This can be understood from Fig. 2 or Fig. 3, which explicitly shows that higher-order corrections reinforce the intensity of the axial field when $t_0 \leq T_0$, which is beneficial for electron energy gain. The energy gains with different order corrections of the ASA solution coincide with each other when corrections become negligibly small when $t_0 > T_0$. One also notices that the electron energy gain obtained with the ASA solution is much larger than that obtained with the PA solution even if the beam waist size is relatively large, especially between $3\lambda_0$ and $20\lambda_0$. This can also be understood from Fig. 1, and Fig. 2 or Fig. 3, which all show that the axial electric field intensity of ASA solution is always larger than that of PA solution as long as the beam waist size is not too small.

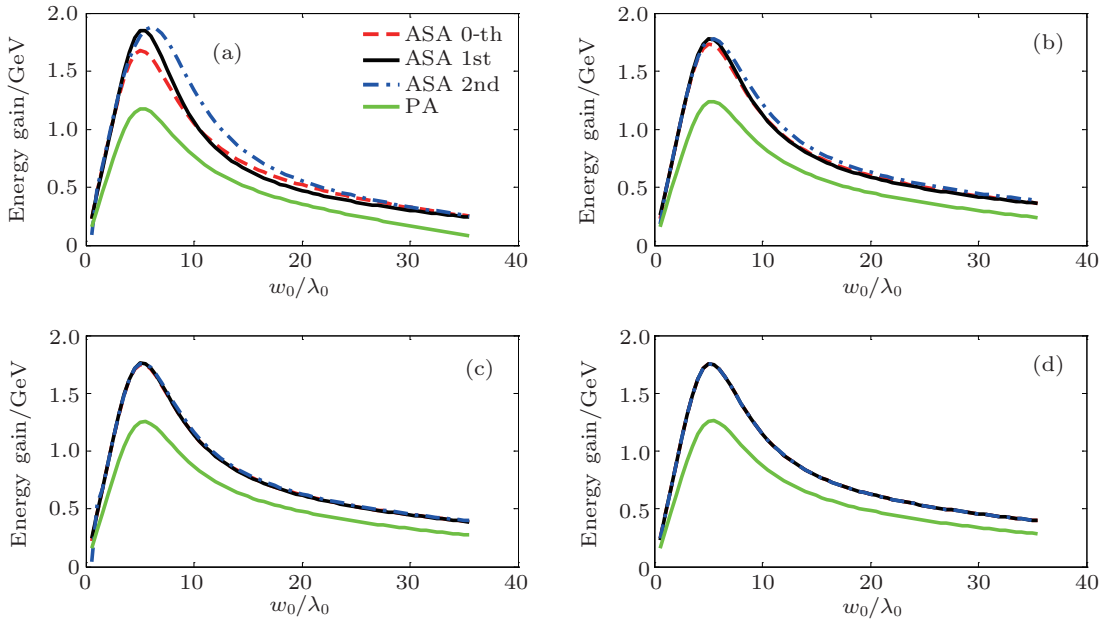


Fig. 5. (colour online) Electron energy gains each as a function of the waist spot size radius w_0 for different pulse durations: $t_0 = 0.25T_0$ (a), $t_0 = 0.5T_0$ (b), $t_0 = T_0$ (c) and $t_0 = 10T_0$ (d). The dimensionless electric field intensity is $E_0 = 100$ and the initial phase of the laser field is $\phi_0 = \pi$. The symbols represent the same meanings as those in Fig. 2.

Figure 6 displays the electron energy gain versus pulse duration t_0. We compare the cases with different diameters $w_0 = 2\lambda$ and $w_0 = 20\lambda_0 = 20$ μm. It shows that the electron energy gain is almost the same for pulse durations $t_0 \geq 2T_0$ regardless of the choice of the axial electric field forms with different orders of correction for the ASA solution. As long as $t_0 < 2T_0$, the energy gain appears different with different orders of temporal correction, in particular with sub-cycle pulses. Usually the energy gain increases with the laser pulse duration increasing. However, for the solution with second-order correction, the generation gain remains as high as that for pulses with $t_0 \geq 2T_0$. This suggests that it is important to keep the high-order temporal correction for pulse duration $t_0 < 2T_0$. Furthermore, a comparison between Figs. 6(a) and 6(b) shows that too large spot sizes are detrimental to electron acceleration, which coincides with the result in Fig. 5.

Figure 7 exhibits the electron energy gain versus the initial position of the laser pulse z_l, where the test electron is located at $z = 0$. In this case, τ in Eq. (12) should be written as $\tau = t - (z - z_l)/c$ and z_l should be a negative value, i.e., the laser pulse propagates a certain distance before catching up with the test electron. Figure 7(a) shows that the energy gain decreases rapidly as the initial position of the laser pulse deviates from $z = 0$ if the pulse is sub-cycle. This is because the axial field rapidly attenuates with the propagation of the laser pulse increasing as shown in Fig. 3. As the initial position of the laser pulse is far from the test electron, its energy gain becomes fixed, which is determined by the asymmetric temporal profile of the laser field, or the initial phase $G \sim -e\int E_z \mathrm{d}z \propto E\sin(\phi)$, because the electron energy gain equals the integration of the electric field that the electron feels along its trajectory, similar to the ponderomotive force acceleration by a sub-cycle linearly-polarized laser pulse discussed in Ref. [16]. It is thus obvious that the energy gain increases linearly with the laser amplitude increasing, which is also confirmed by our numerical calculation. For a laser pulse with a relatively long duration, the electron energy gain varies periodically with the initial position of the laser pulse as shown in Fig. 7(b). When it is initially out of the laser pulse region, the energy gain simply reduces to zero. Changing the initial position of the laser pulse amounts physically to changing the initial phase that the electron initially feels, thus the electron energy gain changes periodically with the changing of z_l. When the electron is initially out of the laser pulse, the integration $G \sim -e\int E_z \mathrm{d}z = 0$ for a multi-cycle pulse. Therefore with multi-cycle pulses, it is hard to obtain high energy electrons from direct laser acceleration experimentally because it is hard to put test electrons in the centre of the laser focus initially.

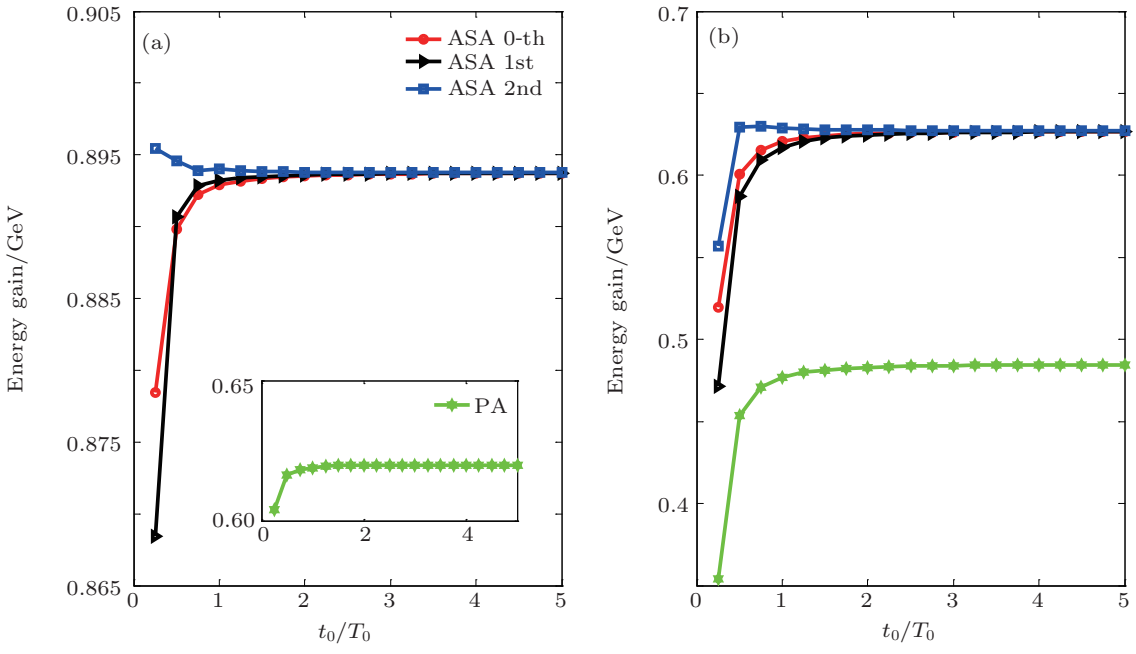


Fig. 6. (colour online) Electron energy gains each as a function of the pulse duration t_0. The dimensionless electric field intensity is $E_0 = 100$, the field initial phase is $\phi_0 = \pi$ and the spot sizes are $w_0 = 2\lambda_0 = 2$ μm (a) and $w_0 = 20\lambda_0 = 20$ μm (b). The initial position of the test electron is at $z = 0$. The symbols represent the same meanings as those in Fig. 2.

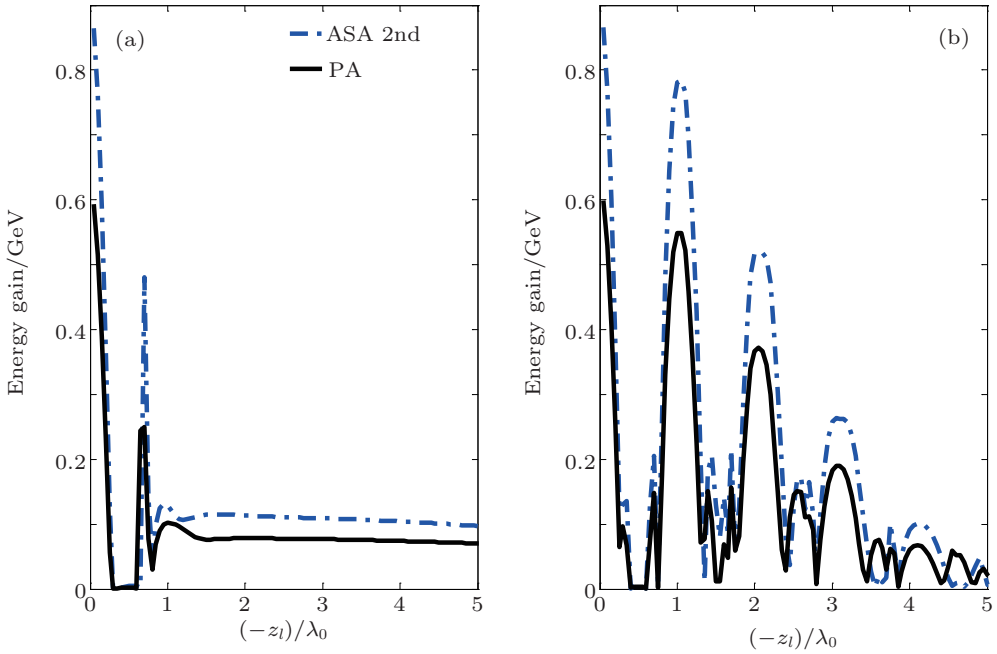


Fig. 7. (colour online) Electron energy gains each as a function of the initial position of the laser pulse away from its focus at $z = 0$, where the test electron is located. The dimensionless electric field intensity is $E_0 = 100$, the field initial phase is $\phi_0 = \pi$ and the spot size is $w_0 = \lambda_0 = 2$ μm. The laser pulse durations are $t_0 = 0.5T_0$ (a) and $t_0 = 2T_0$ (b), respectively. The symbols represent the same meanings as those in Fig. 2.

5. Summary

In this paper, we proposed a solution for the propagation of radially polarized few-cycle laser pulse in vacuum according to the angular plane-wave spectrum analysis (ASA) of the electromagnetic fields. A comparison between this ASA solution and the paraxial approximation (PA) solution for describing electron acceleration was made. It is found that there is significant difference between the energy gain obtained with the non-paraxial solution and that obtained with the paraxial results even if the beam waist size is much larger than laser wavelength. It is also found that the spatial and the temporal couplings of the laser pulse profiles also have a strong effect on the electron energy gain.

References

[1] Strickland D and Mourou G 1985 *Opt. Commun.* **264** 219

[2] Perry M D, Pennington D, Stuart B C, Tietbohl G, Britten J A, Brown C, Herman S, Golick B, Kartz M, Miller J, Powell H T, Vergino M and Yanovsky V 1999 *Opt. Lett.* **24** 160

[3] Salamin Y I 2006 *New J. Phys.* **8** 133

[4] Martinez-Herrero R, Mejias P M and Bosch S 2008 *Opt. Commun.* **281** 3046

[5] Martinez-Herrero R, Mejias P M and Manjavacas A 2010 *Appl. Phys.* B **99** 579

[6] Deng D M and Guo Q 2007 *Opt. Lett.* **18** 2711

[7] Liu M P, Wu C, Xie B S, Liu J, Wang H Y and Yu M Y 2008 *Phys. Plasmas* **15** 023108

[8] Salamin Y I 2006 *Phys. Rev.* A **73** 043402

[9] Salamin Y I 2007 *Opt. Lett.* **32** 90

[10] Gupta D N, Kumar S, Yoon M, Hur M S and Suk H 2007 *Phys. Lett.* A **368** 402

[11] Kunwar P S and Kumar M 2011 *Phys. Rev. ST Accel. Beams* **14** 030401

[12] Davis L W 1979 *Phys. Rev.* A **19** 1177

[13] Lax M, Louisell W H and Mcknight W B 1975 *Phys. Rev.* A **11** 1365

[14] Lin Q, Zheng J and Becker W 2006 *Phys. Rev. Lett.* **97** 253902

[15] Agrawal G P and Lax M 1979 *J. Opt. Soc. Am.* **69** 575

[16] Rau B, Tajima T and Hojo H 1997 *Phys. Rev. Lett.* **78** 3310

[17] Brice Q and Mora P 1998 *Phys. Rev.* E **58** 3719

[18] Liu J L, Sheng Z M and Zheng J 2011 *Opt. Commun.* **281** 3046.

[19] Hua J F, Ho Y K, Lin Y Z, Chen Z, Xie Y J, Zhang S Y, Yan Z and Xu J J 2004 *Appl. Phys. Lett.* **85** 3705

[20] Xie Y J, Ho Y K, Kong Q, Wang P X, Chen Z and Liu J R 2006 *Chin. Phys. Lett.* **23** 599

[21] Zhang J T, Wang P X, Kong Q, Chen Z and Ho Y K 2007 *Nucl. Instrum. Method* A **580** 1169